Clays and Clay Minerals, Vol. 58, No. 4, 501–514, 2010.

HYDROTHERMAL STABILITY OF LAYERED SILICATES IN NEUTRAL AND ACIDIC MEDIA: EFFECT ON ENGINEERED-BARRIER SAFETY

María D. Alba[1,*], Miguel A. Castro[1], Pablo Chain[1], M. Mar Orta[1], M. Carolina Pazos[2], and Esperanza Pavón[1]

[1] Departamento de Química Inorgánica, Instituto Ciencia de los Materiales de Sevilla, CSIC-Universidad de Sevilla, Avda. Américo Vespucio, 49, 41092-Sevilla, Spain

[2] Laboratorio de Catálisis Heterogénea, Departamento de Química, Universidad Nacional de Colombia, A.A. 14490, Bogotá, D.C., Colombia

Abstract—Many environmental applications in the inorganic remediation field are based on the swelling and ion-exchange capacities of smectites, even though these can be affected by hydrothermal treatment in water and acidic media. Here a systematic study of the properties of layered silicates that could affect their hydrothermal stability at different pH is described: type of layers, octahedral occupancy, layer charge, and origin of the layer charge. The silicates studied were selected on the basis of their different characteristics associated with these properties. Kanemite (1:0 phyllosilicate), kaolinite (1:1 phyllosilicate), and pyrophyllite and talc (2:1 phyllosilicates with no-layer charge) were examined in order to determine the effect of layer structure, whereas the hydrothermal reactivity of silicates with different layer charge was analyzed by comparing the talc-hectorite-Laponite® and talc-saponite-trioctahedral vermiculite series. Samples were treated hydrothermally at 300ºC for 48 h in pure water and in a 0.01 M HNO_3 solution and the final products were analyzed by X-ray diffraction, scanning electronic microscopy, and solid-state nuclear magnetic resonance spectroscopy. All layered silicates, except for kanemite, were found to remain intact after hydrothermal treatment in water and acidic media, with only minimal short-range structural changes observed. The extent of the structural changes depended on the octahedral sheet occupancy (greater extent) and the number of isomorphic substitutions (lesser extent), both of which weaken the structure.

Key Words—Bentonite, Engineered-barrier, Hydrothermal Stability, Layered Silicates,

INTRODUCTION

Natural and modified bentonites, which consist mainly of smectites, have been used in many applications (Grim, 1968; Grim and Güven, 1978; Murray, 1991, 1999, 2000; Bergaya *et al.*, 2006). Bentonite, especially Na-bentonite, is used extensively either on its own or as a component in soil mixtures in many geoenvironmental engineering applications, including the construction of waste-containment barriers. The design of such barriers requires the compatibility of the soil barrier with the waste. The main hurdle to overcome during the design and construction of safe nuclear-waste repositories is that of water, which can transport the radionuclides in dissolved form or as colloids or small particles. If water reaches the canister and corrodes it, the emplacement should be able to retain the radionuclides in the water and avoid their transport away from the repository (Cuadros, 2008). The interaction of this barrier material with groundwater can, however, modify its physical and chemical properties, thus decreasing its groundwater isolation capacity or, in the case of canister failure, decreasing the radionuclide retention capacity of clay materials (Pusch *et al.*, 2007).

Because accidents can modify the behavior of such barriers, the hydrothermal stability of clay in water and in basic and acidic media is of great importance, particularly where radioactive-waste confinement is concerned. In many countries (such as Belgium, Germany, France, Japan, Switzerland, *etc.*), deep clay formations are considered to be potential host rocks for radioactive-waste disposal and so the clay buffer is of special concern because even moderate mineralogical changes can lead to the reduction and, eventually, to the loss of the critical sealing and mechanical properties of the buffer (Pusch and Yong, 2003; Pusch *et al.*, 2003). Precise knowledge of the clay's properties in the various domains concerned with construction feasibility, such as the long-term integrity of the bentonite as it comes into contact with either acidic tailings pore water (in the case of slurry wall, filter cake) or acidic, stored, mine water (in the case of acid-mine drainage, collection ponds), is, therefore, of crucial importance when assessing the performance and safety of radioactive-waste disposal concepts. Furthermore, concrete and cement, which have been proposed for use as matrix material, backfill material, and structural components of radioactive-waste repositories (Glasser, 2001), are likely to produce solutions with a high pH which will also modify the clay's properties.

* E-mail address of corresponding author:
alba@icmse.csic.es
DOI: 10.1346/CCMN.2010.0580405

The hydrothermal stability of smectites has been studied extensively, although much of this work has centered on the collapse of expandable smectites to non-expandable layered silicates, in particular the formation of illite (Jennings and Thompson, 1986; Cuadros, 2008). The transformation of clay minerals as a consequence of concrete and cement degradation has also been studied extensively (Read *et al.*, 2001; Savage *et al.*, 2002; Ramírez *et al.*, 2002; Mantovani *et al.*, 2009). Acid treatment of clay minerals is used widely in both research and industrial applications (Siddiqui, 1968; Gregor and Čičel, 1969; Fahn & Fenderl, 1983; Morgan *et al.*, 1985; Adams, 1987). Indeed, the acidity of acid centers on various forms of smectites has been found to affect their sorption properties significantly (Breen *et al.*, 1987; Breen, 1988, 1991a, 1991b; Jovanovič and Janačkovič, 1991), and the acid dissolution of clays has provided useful information regarding the reactivity of the mineral involved, such as kinetic parameters (Čičel and Novak, 1977; Novak and Čičel, 1978; Corma *et al.*, 1990; Cetisli and Gedikbey, 1990; Güler and Sarier, 1990), or the characteristics of the reactants and reaction products (Čičel *et al.*, 1965; Fahn, 1973; Garcia *et al.*, 1989). Although numerous data exist regarding cation leaching and the weathering of alumino-silicates under acidic conditions (Nagy, 1995), only limited information exists on the transformation of smectites in acidic solution (Bauer *et al.*, 2001), despite its importance in terms of the stability of clay barriers in radioactive-waste repositories.

The aim of the present research was to study the properties of layered silicates, in particular layer type, octahedral occupancy, layer charge, and origin of the layer charge, that could affect their hydrothermal stability in two different media, namely water and strong acid. A series of silicates with different sets of characteristics was chosen. Kanemite, which has only one tetrahedral sheet (referred to below as neutral 1:0 phyllosilicate), kaolinite (1:1 phyllosilicate), and pyrophyllite and talc (2:1 phyllosilicates with no layer charge) were chosen to determine the effect of the layer structure. Talc and pyrophyllite have trioctahedral and dioctahedral structures, respectively, and were studied to determine the influence of the degree of octahedral occupancy on the hydrothermal stability. The hydrothermal reactivity of silicates with different layer charge was analyzed by comparing the talc-hectorite-Laponite® and talc-saponite-trioctahedral vermiculite series. A comparison of talc and saponite, where the charge originates from isomorphic substitutions in the tetrahedral sheet, and hectorite and Laponite®, where the charge originates from isomorphic substitutions in the octahedral sheet, allows the hydrothermal stability to be related to the origin of the silicate layer charge.

EXPERIMENTAL METHODS

Material

Starting materials. Eight well characterized phyllosilicates were selected for study (structural formulae in Table 1), one of which was a 1:0 phyllosilicate, another a 1:1 phyllosilicate, with the rest having a 2:1 layer structure. The 1:0 phyllosilicate selected was a synthetic kanemite, $Na[Si_2O_4(OH)].3H_2O$, which is a layered silicate containing only one sheet of orthosilicate tetrahedra. The orthosilicate groups are condensed into three of its vertices (Q^3) in an irregular hexagonal arrangement. The silicate sheets are bound by hydrogen bonds and hydrated Na^+ cations interact closely with the hydroxyl groups of the sheets in the interlayer space. A more detailed structural description of this silicate can be found elsewhere (Alba *et al.*, 2006). A low-defect kaolinite was chosen as the 1:1 phyllosilicate (White *et al.*, 1992). The 2:1 phyllosilicates selected included dioctahedral and trioctahedral layered silicates pyrophyllite and talc, respectively, which are almost free of layer charge; three trioctahedral smectites (saponite, hectorite, and Laponite®); and one trioctahedral vermiculite, namely eucatex (Williams-Daryn *et al.*, 2002).

Table 1. Layered aluminoslicates used as starting material.

Silicate	Source	Chemical formulae
Kanemite[1]	Synthetic[a]	$Na[Si_2O_4(OH)]\cdot 3H_2O$
Pyrophyllite[2]	Natural Hillsboro	$(Ca_{0.006}Na_{0.012}K_{0.018})[Si_4][Al_{1.95}Fe_{0.01}Ti_{0.005}Mg_{0.001}]O_{10}(OH)_2$
Talc[3]	Natural Lillo	$[Si_4][Mg_{2.95}Fe_{0.017}]O_{10}F_{0.19}(OH)_{1.81}$
Kaolinite[4]	Low-defect Natural Washington County	$Na_{0.01}K_{0.01}Ca_{0.01}Mg_{0.02}[Si_{3.83}Al_{0.17}][Al_{3.86}Fe_{0.02}Ti_{0.11}]O_{10}(OH)_8$
Hectorite[5]	Natural[b] S. Bernardino	$Ca_{0.17}[Si_{3.98}Al_{0.02}][Mg_{2.65}Al_{0.02}Li_{0.33}]O_{10}(OH)_2$
Laponite®[6]	Synthetic[c]	$Na_{0.35}[Si_4][Mg_{2.73}Li_{0.2}]O_{10}(OH)_2$
Saponite[7]	Natural[b] California	$Na_{0.31}K_{0.01}Ca_{0.04}[Si_{3.6}Al_{0.4}][Mg_{2.9}Fe_{0.07}]O_{10}(OH)_2$
Vermiculite[8]	Natural Eucatex	$Na_{0.7}[Si_{3.1}Al_{0.9}][Mg_{2.48}Al_{0.08}Fe_{0.31}Ti_{0.04}Mn_{0.01}]O_{10}(OH)_2$

[a] synthesized by Alba *et al.* (Alba *et al.*, 2006); [b] Source Clays Repository of The Clay Minerals Society; [c] Solvay Alkali GMBH

[1] Alba *et al.* (2006); [2] Sánchez Soto *et al.* (1994); [3] Petit *et al.* (2004); [4] White *et al.* (1992); [5] Laporte Industries Ltd (1990), Levitz *et al.* (2000); [6] Prost (1984); Alba *et al.* (2001a, 2001b); [7] Ames *et al.* (1958); [8] Williams-Daryn *et al.* (2002)

https://doi.org/10.1346/CCMN.2010.0580405 Published online by Cambridge University Press

Two of these silicates (vermiculite and saponite) contain Al substituting for Si in the tetrahedral sheet of the clay, whereas the rest contain only Si in the tetrahedral sheet. Finally, hectorite and Laponite® contain Li substituting for Mg in the octahedral sheet and differ in their degree of crystallization, which is poorer in Laponite® than in hectorite. Original samples with particle diameters of <2 μm were used, after removal of carbonates and organic matter.

Hydrothermal treatments. 300 mg of the powdered silicate and 50 mL of distilled water or 0.01 M HNO_3 solution were transferred into a stainless steel T316SS hydrothermal reactor and heated up to 300ºC for 48 h after which time the reactor was cooled to room temperature and the solids separated by filtration, washed repeatedly with distilled water, and allowed to dry in air at 25ºC. Although geochemical waste degradation and waste/rock interaction processes in the hydrothermal environment remain predictable up to temperatures of ~200ºC, many studies devoted to simulating deep geological disposal conditions use temperatures of up to 350ºC to increase reaction rates (Mather *et al.*, 1982; Savage and Chapman, 1982; Allen and Wood, 1988; Alba and Chain, 2007).

Experimental techniques

X-ray powder diffraction. X-ray diffraction (XRD) patterns were obtained using a Bruker D8I instrument, at CITIUS (Centre of Research, Technology and Innovation of Seville University), University of Seville, Spain. The instrument works with Ni-filtered CuKα radiation at 40 kV and 40 mA. The XRD patterns were obtained over the range 3−70º2θ at a step size of 0.05º2θ and a counting time of 3 s.

Scanning electron microscopy (SEM). The morphology and chemical compositions of the samples were analyzed at the Microscopy Service of the Instituto Ciencia de los Materiales de Sevilla (CSIC-US) with a Scanning Electron Microscope (JEOL JSM 5400) equipped with a LINK Pentafet probe and ATW windows for Energy Dispersive X-ray Analysis (EDX). The powder samples were coated with a gold film to a thickness of 2−3 nm using an Emitech K550 coater system (Instituto Ciencia de los Materiales de Sevilla (CSIC-US), Sevilla, Spain).

Nuclear magnetic resonance spectroscopy (MAS NMR). ^{29}Si, ^{27}Al, and ^{1}H single-pulse spectra were recorded using a Bruker DRX400 spectrometer with a magnetic field of 9.36 T and equipped with a multinuclear probe of the Spectroscopy Service of CSIC-US. Powdered samples were packed in 4 mm zirconia rotors and spun at 12 kHz. ^{1}H MAS NMR spectra were obtained at a frequency of 400.13 MHz using a typical π/2 pulse width of 4.5 μs and a pulse space of 5 s. The ^{29}Si MAS NMR spectra were obtained at a frequency of 79.49 MHz using a π/6 pulse width of 2.7 μs and a pulse space of between 60 and 600 s. ^{27}Al MAS NMR spectra were recorded at 104.26 MHz with a π/20 pulse width of 1.1 μs and delay time of 3 s. The chemical shifts are reported in ppm from tetramethylsilane for ^{29}Si and ^{1}H and from 0.1 M solutions of $AlCl_3$ for ^{27}Al. The spectra were simulated using a modified version of the Bruker *Winfit* program to handle the finite spinning speed in MAS experiments (Massiot *et al.*, 2002). A Gaussian−Lorentzian model was used for all the peaks. The parameters fitted were intensity, position, linewidth, and Gaussian/Lorentzian ratio.

RESULTS

Phyllosilicates with non-layer charge

The XRD patterns of kanemite (Figure 1a) consisted of a set of reflections corresponding to those of the standard kanemite structure PDF 25-1309 with a 020 basal spacing of 10.2 Å (Johan and Maglione, 1972), but all disappeared after hydrothermal treatment in water and an acidic medium (Figure 1b,c). Instead, the patterns were similar to tridymite (PDF 03-0227) and cristobalite (PDF 03-272) as decomposition products in both cases.

The XRD pattern of the kaolnite (Figure 1a) was indexed according to the standard kaolinite pattern PDF 12-0447, with a basal spacing of 7.2 Å. Hydrothermal treatments in water (Figure 1b) and acidic solution (Figure 1c) did not alter the structure, *i.e.* the basal spacing of the starting material remained the same.

The XRD pattern of pyrophyllite (Figure 1a) was indexed according to the PDF 46-1308 pattern, with a basal spacing of 9.1 Å. Hydrothermal treatments in water (Figure 1b) and acidic solution (Figure 1c) did not alter the structure, crystallinity, or the collapsed state of the layers, which maintained the basal spacing of the starting material. The emergence of a new reflection at 14.6º2θ was observed in both XRD patterns and corresponded to boehmite (PDF 76-1871), which was previously observed as a product of hydrothermal treatment of beidellite and muscovite at 300ºC, thus indicating that this structure shows some stability under hydrothermal conditions (Bentabol *et al.*, 2003).

The XRD pattern of talc (Figure 1a) was indexed according to PDF 29-1494, with a basal spacing of 9.2 Å due to its non-swelling layered silicate. The XRD patterns of the treated samples (Figure 1b,c) were identical to those of the untreated sample. A detailed analysis revealed the absence of reflections resulting from new crystalline phases and, therefore, the crystalline state of talc was unchanged by the treatment.

Analysis of the samples by MAS NMR and SEM/EDX was carried out to determine the presence of any change in short-range order. The ^{29}Si MAS NMR spectra of the starting materials and those obtained after the hydrothermal treatments (Figure 2, Table 2) revealed for

https://doi.org/10.1346/CCMN.2010.0580405 Published online by Cambridge University Press

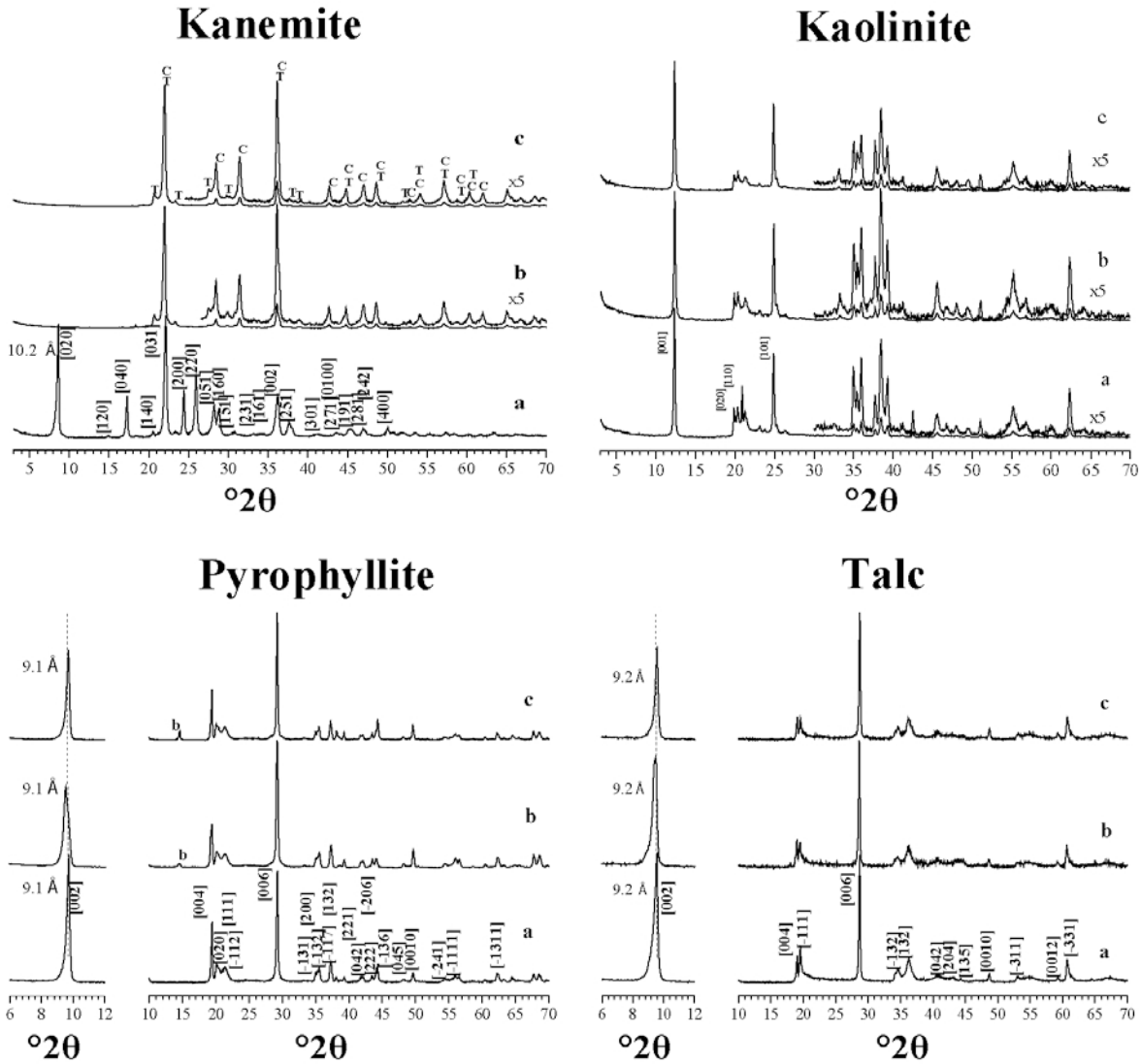

Figure 1. XRD patterns of kanemite, kaolinite, pyrophyllite, and talc: (a) starting materials, and after hydrothermal treatment at 300ºC for 48 h in two different chemical media; (b) water; and (c) 0.01 M HNO_3 solution. C = cristobalite, T = tridymite, and b = boehmite.

kanemite a unique signal centered at −97.3 ppm due to some condensation of Q^3 silicon tetrahedra, typical of this silicate (Blasco *et al.*, 1985). The spectra of treated samples showed two signals at −109 ppm and −111 ppm, The chemical shifts were assigned to environments $Q^4(0Al)$ of cristobalite and tridymite, which presented a set of signals between −109.0 and −113.0 ppm with a maximum at −111.0 ppm, respectively (Engelhardt and Michel, 1987). This finding was in good agreement with the XRD data.

The ^{29}Si NMR spectrum of kaolinite (Figure 2, Table 2) showed a signal at −91.5 ppm, which corresponds to a Q^3 coordination sphere with no condensation of Al atoms in the neighboring tetrahedra, Q^3 (0Al) (Engelhardt and Michel, 1987). The spectra recorded after hydrothermal treatments showed two signals, one in the Q^3 resonance range and another new signal at higher frequency (between −87.1 and −89.8 ppm), corresponding to a lower condensation degree of the Si tetrahedra (Engelhardt and Michel, 1987). Both hydrothermal treatments provoked a broadening of the Si signal due to a short-range disorder of the Si environment, which was greater after water treatment. In contrast, the relative intensity of the new signal, at greater frequency, was greater after the acid treatment than after the water treatment.

The ^{29}Si NMR spectrum of pyrophyllite (Figure 2, Table 2) showed a signal at −95.2 ppm, corresponding to a Q^3 coordination sphere without condensation of Al atoms in the neighboring tetrahedra, Q^3 (0Al) (Engelhardt and Michel, 1987). The spectra recorded after hydrothermal treatments of the original pyrophyllite showed a

https://doi.org/10.1346/CCMN.2010.0580405 Published online by Cambridge University Press

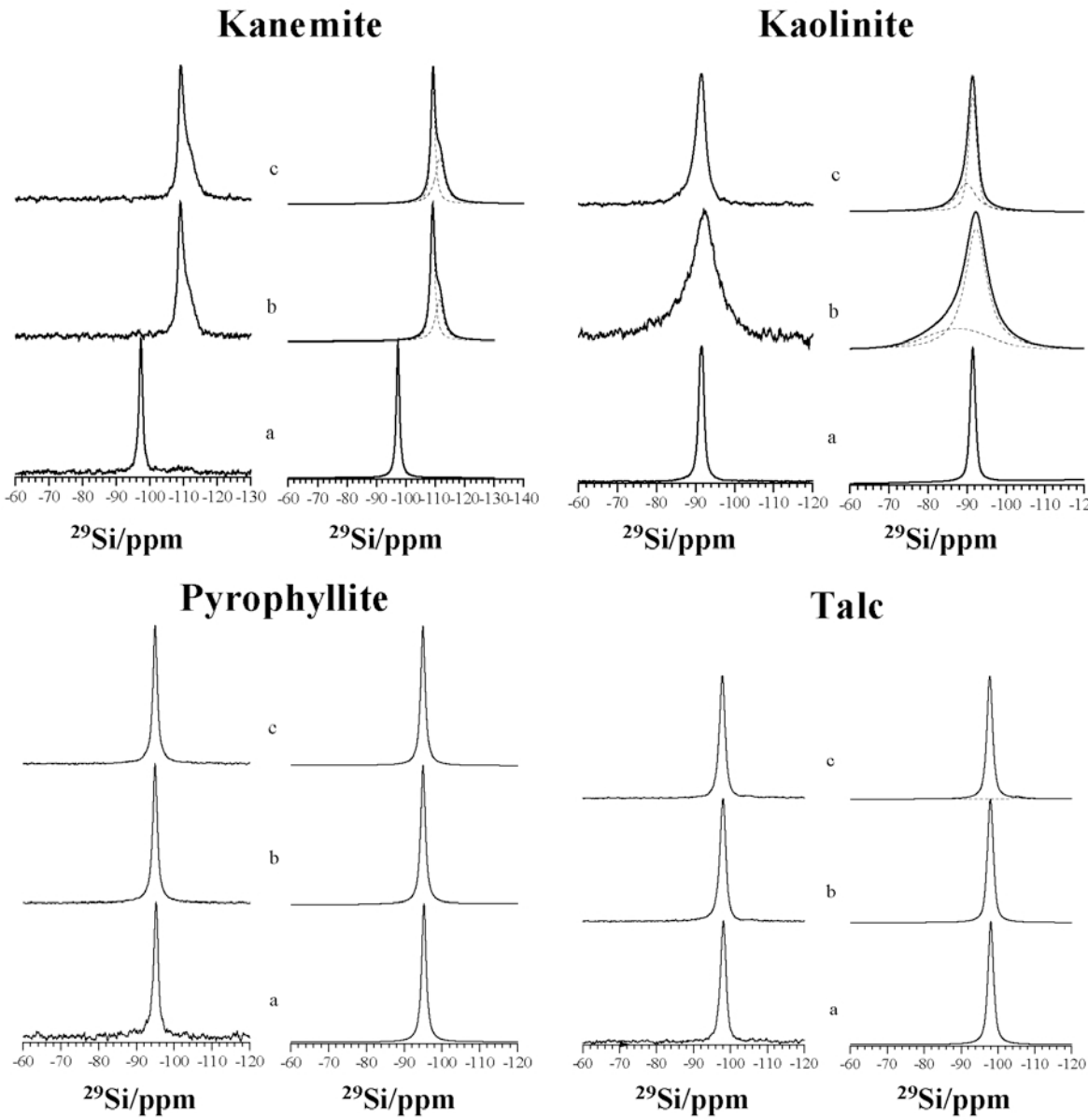

Figure 2. ^{29}Si MAS NMR spectra and fits of kanemite, kaolinite, pyrophyllite, and talc: (a) starting materials, and after hydrothermal treatment at 300ºC for 48 h in two different chemical media; (b) water; and (c) 0.01 M HNO_3 solution.

single contribution in the same position as for the untreated sample. The signal of the sample treated with water was, however, broader than that for the untreated sample, which may indicate the loss of short-range order. No appreciable change in signal width was observed when the sample was treated in an acidic medium. Finally, talc showed a single contribution to the ^{29}Si NMR spectrum at −98.1 ppm, due to $Q^3(0Al)$ (Sanz and Serratosa, 1984). The single peak in the spectrum of the sample treated hydrothermally in water showed no significant change in its chemical shift, although it was significantly broader due to a decrease in the short-range order. The talc ^{29}Si signal at −97.8 ppm shifted toward higher frequencies (higher ppm values) upon hydrothermal treatment in an acidic medium, possibly as a result of vacancies in the octahedral sheet generated by Mg^{2+} leaching (Sanz and Serratosa, 1984). A lesser peak at −105.6 ppm, resulting from Si in a Q^4 environment, was also observed. Mg^{2+} leaching from the octahedral sheet during the treatment was also evident from the shift of the hydroxyl ^{1}H NMR signal (not shown) toward lower frequency (Alba *et al.*, 2003).

The ^{27}Al MAS NMR spectra of the untreated kaolinite and pyrophyllite (the only two samples with framework Al) and those recorded after the hydrothermal treatments were identical, with a single peak at

https://doi.org/10.1346/CCMN.2010.0580405 Published online by Cambridge University Press

Table 2. ^{29}Si chemical shift, FWHM, and area under the curve of the different contributions obtained from the fitting of the ^{29}Si MAS NMR spectrum of kanemite, kaolinite, pyrophyllite, and talc

δ (ppm)	FWHM (Hz)	%	Phase
Kanemite			
Starting material			
−97.3	99	100	Q^3(0Al)
After hydrothermal treatment in water			
−109.1	137	60.8	Q^4(0Al) cristobalite
−111.4	266	39.2	Q^4(0Al) tridymite
After hydrothermal treatment in 0.01 M HNO_3 solution			
−109.2	131	52.8	Q^4(0Al) cristobalite
−111.5	305	47.2	Q^4(0Al) tridymite
Kaolinite			
Starting material			
−91.5	126	100	Q^3(0Al)
After hydrothermal treatment in water			
−87.7	1444	23.5	low condensed phase
−92.3	530	76.5	Q^3(0Al)
After hydrothermal treatment in 0.01 M HNO_3 solution			
−89.8	463	40.1	low condensed phase
−91.5	198	59.9	Q^3(0Al)
Pyrophyllite			
Starting material			
−95.2	111	100	Q^3(0Al)
After hydrothermal treatment in water			
−94.9	115	100	Q^3(0Al)
After hydrothermal treatment in 0.01 M HNO_3 solution			
−95.0	112	100	Q^3(0Al)
Talc			
Starting material			
−98.1	141	100	Q^3(0Al)
After hydrothermal treatment in water			
−98.0	152	100	Q^3(0Al)
After hydrothermal treatment in 0.01 M HNO_3 solution			
−97.8	145	98.4	Q^3(0Al)
−105.6	209	1.6	Q^4

~0 ppm, due to the octahedral Al environments. These results again suggested the stability of the kaolinite and pyrophyllite structures after both treatments. The formation of boehmite upon treatment of pyrophillite produced no spectral change due to the octahedral coordination of Al in this phase (Engelhardt and Michel, 1987).

The SEM images and EDX spectra of the kanemite before and after hydrothermal treatments revealed that untreated kanemite particles had a laminar appearance (Figure 3a) and intense Si and NaKα EDX peaks (Figure 3d), as would be expected for this silicate. The similarity of the XRD patterns and ^{29}Si NMR spectra of the material after both types of hydrothermal treatments was also found in the SEM/EDX analysis. Thus, both samples consisted of small, round particles (Figure 3b, 3c) and their EDX spectra (Figure 3e, 3f) showed only the SiKα peak.

Textural analysis of the two 2:1 phyllosilicates showed only one type of particle with a laminar appearance and EDX spectra with intense SiKα and AlKα (pyrophyllite) or MgKα (talc) peaks, depending on the chemical composition. The SEM images and associated EDX spectra of the samples treated in water and in acidic medium did not differ from those of the untreated samples. The presence of boehmite in the treated pyrophyllite could not be confirmed by this technique, probably because it is only present as a minor phase.

Charged phyllosilicates

The structural changes in the long-range order of the charged trioctahedral 2:1 phyllosilicates after both types of hydrothermal treatments were analyzed by XRD (Figure 4). All the reflections observed for the initial samples (Figure 4a) were consistent with the general and basal reflections of smectite and vermiculite, except the reflection at ~30º2θ in hectorite, which corresponds to cristobalite (PDF 03−272). The 060 reflections were observed at a 2θ angle that corresponded to a distance

https://doi.org/10.1346/CCMN.2010.0580405 Published online by Cambridge University Press

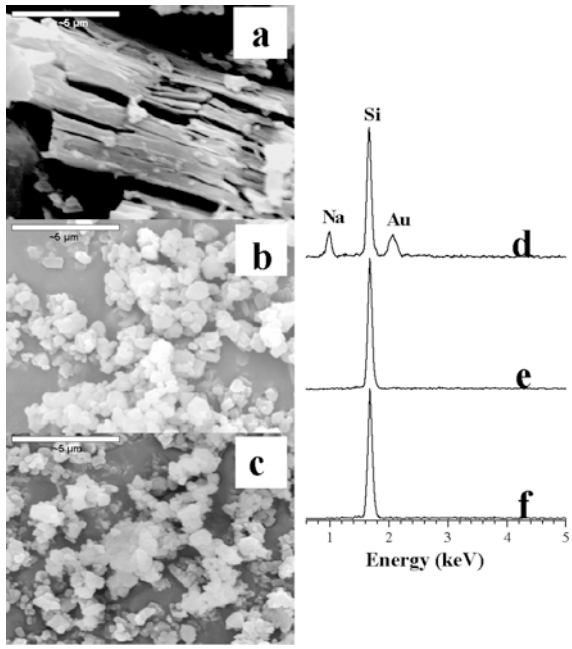

Figure 3. SEM images and EDX spectra of kanemite: (a,d) starting material, and after hydrothermal treatment at 300ºC for 48 h in two different chemical media; (b,e) water; and (c,f) 0.01 M HNO_3 solution.

between the reflection planes of 1.51−1.53 Å, typical of trioctahedral 2:1 phyllosilicates (Alba *et al.*, 2001a). The 001 basal reflection corresponded to a d_{001} value of ~12.0 Å which was assigned to a water monolayer around the interlayer cations (Alba *et al.*, 2001a). The XRD pattern of Laponite® showed broader reflections than the other silicates, mainly due to its smaller particle size, which causes a relative loss of long-range order (Wheeler *et al.*, 2005).

The *hkl* reflections did not change upon hydrothermal treatments (Figure 4b, 4c), thus indicating that the basic structure of the silicates remained intact and that no other crystalline phases were present in the material. However, their positions, widths, and intensities did change due to the effects of the hydrothermal environment on the structure. Thus, hydrothermal treatment in the water medium (Figure 4b) caused a partial swelling of the layers up to 12.5−13.5 Å (smectites) or up to two distances, 12.4 and 14.1 Å (vermiculite). A significant increase in the width of the 001 reflection was observed after this treatment, which could be due to greater heterogeneity in the basal spacing caused by leaching of divalent and trivalent cations from the framework without completely displacing the monohydrated interlayer cations. The exception was Laponite®, the 001 reflection of which narrowed after hydrothermal treatment due to an increase in the long-range order of the layer stacking. The hydrothermal treatment in acidic medium resulted in more dramatic changes than the previous treatment (Figure 4c) with the 001 reflection, which is associated with a *c* parameter of 14.5 Å and reflects the total replacement of the monohydrated interlayer cations by divalent and trivalent cations leached from the framework (Luce and Parks, 1972; Corma *et al.*, 1987). The number and intensity of the basal reflections increased, probably because of a higher-order stacking of the layers after the treatment. In general, all the samples showed good stability with respect to the long-range order which was unaffected by the chemical composition of the silicates analyzed.

The changes in short-range order produced by the two hydrothermal treatments were followed by MAS NMR spectroscopic analysis of the active nuclei present in each silicate (Figure 5, Tables 3 and 4). The only major signal in the ^{29}Si NMR spectrum of untreated hectorite (Table 3) was a peak in the range of chemical shifts associated with the Q^3 (0Al) environment. The shift of the signal at −95.0 ppm to higher frequencies with respect to talc was due to the isomorphic substitution of Li^+ for Mg^{2+} in the octahedral sheet, which resulted in a decrease in the electronegativity of the cations coordinated by the apical oxygen of the tetrahedral sheet (Weiss *et al.*, 1987). Acid treatment resulted in no significant structural changes, with the position and width of the Q^3(0Al) signal remaining at values similar to those found for the untreated sample. In contrast, hydrothermal treatment in water led to an increase in the local disorder around the Si, which resulted in a significantly broader signal than that of the untreated sample (FWHH 302 Hz *vs.* 239 Hz in the starting material). The shift of the signal to higher frequency in both treatments may be due to the creation of octahedral vacancies upon leaching of framework cations (Sanz and Serratosa, 1984).

The spectrum of initial Laponite® (Table 3) was characterized by a main signal at −94.5 ppm assigned to a Q^3(0Al) environment, along with a shoulder at −97.3 ppm and a minor peak at −85.2 ppm. The main signal shifted to greater frequencies with respect to that for hectorite due to the increased layer-charge deficit in Laponite® (Weiss *et al.*, 1987). The signal at −97.3 ppm was due to the presence of partially condensed Si tetrahedra with anionic basal oxygens, $(SiO)_3SiO^-$ (Wheeler *et al.*, 2005), whereas the higher-frequency signal was assigned to silanol groups, $(SiO)_3SiOH$ (Wheeler *et al.*, 2005). Both treatments produced an increase in the intensity of the signal at ~−97.0 ppm along with a concomitant decrease in the intensity of the main signal at ~−94.5 ppm, a phenomenon which could be explained by an increase in the partially condensed Si in the tetrahedral sheet of hydrothermal treatments. Acid treatment also produced a new small signal (7.4%) at −95.1 ppm which was in the Q^3(0Al) range but shifted to a greater frequency than the Q^3(0Al) signal of untreated Laponite®. The new signal might have arisen due to the creation of octahedral vacancies upon

https://doi.org/10.1346/CCMN.2010.0580405 Published online by Cambridge University Press

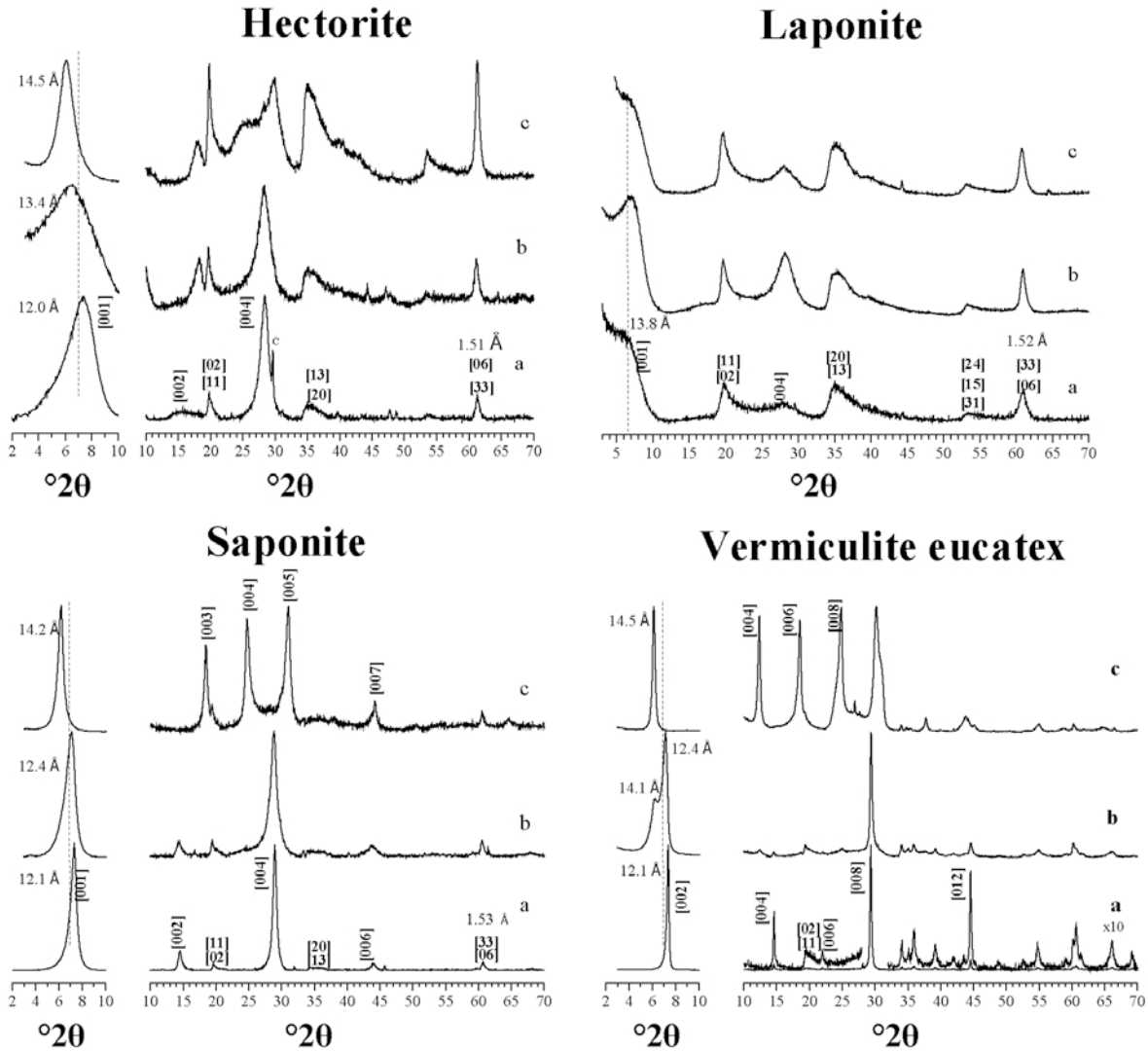

Figure 4. XRD pattern of hectorite, Laponite®, saponite, and vermiculite eucatex: (a) starting materials, and after hydrothermal treatment at 300ºC for 48 h in two different chemical media; (b) water; and (c) 0.01 M HNO_3 solution. C = cristobalite.

leaching of framework cations (Sanz and Serratosa, 1984).

The ^{29}Si MAS NMR spectrum of the untreated saponite showed a signal with three contributions (Table 4); an intense signal at −95.8 ppm and two lower-intensity signals at −90.8 and −85.0 ppm, corresponding to Q^3(0Al), Q^3(1Al), and Q^3(2Al) Si environments, respectively (Alba *et al.*, 2001b). Calculation of the Si/Al ratio gave values of 8.9, very close to the theoretical value of 9.0 obtained from the chemical formula. The similarity between the spectra of treated and untreated samples indicates that the ^{29}Si environments did not change substantially upon hydrothermal treatment. Mathematical treatment of the three spectra revealed that the sample treated hydrothermally in water had broader signals indicative of an increased local disorder around Si. Furthermore, the treatment caused a slight increase in the Si/Al ratio to 10.0, possibly due to a partial leaching of Al from the tetrahedral sheet.

The ^{29}Si NMR signals obtained for vermiculite (Table 4) were abnormally broad due to the presence of Fe in its structure. The single signal with a maximum at −88.5 ppm, due to Q^3 environments, observed for the untreated sample could be fitted to four peaks (Table 4). The small Si/Al ratio in this silicate (3.5) resulted in a greater contribution of $Q^3(m\text{Al})$ with $m \neq 0$ environments to the ^{29}Si signal than in the smectites. Neither hydrothermal treatment shifted the maximum of the broad signal in the spectrum significantly, although they both produced an increase in the bandwidth and a decrease in the relative intensity of the Q^3(mAl)/Q^3(0Al) signals as a result of the effect of short-range structural disorder and partial leaching of Al.

https://doi.org/10.1346/CCMN.2010.0580405 Published online by Cambridge University Press

Table 3. ^{29}Si chemical shift, FWHM, and area under the curve of the different contributions obtained from the fitting of the ^{29}Si MAS NMR spectrum of hectorite and Laponite®.

δ (ppm)	FWHM (Hz)	%	Phase
Hectorite			
Starting material			
−95.0	239	100	Q^3(0Al)
After hydrothermal treatment in water			
−94.7	302	100	Q^3(0Al)
After hydrothermal treatment in 0.01M HNO_3 solution			
−94.8	234	100	Q^3(0Al)
Laponite®			
Starting material			
−97.3	188	13.3	Q^3(0Al), $(SiO)_3SiO^-$
−94.5	263	79.0	Q^3(0Al)
−85.2	316	7.7	Q^3(0Al), $(SiO)_3SiOH$
After hydrothermal treatment in water			
−97.0	274	48.7	Q^3(0Al), $(SiO)_3SiO^-$
−94.2	221	45.9	Q^3(0Al)
−85.8	208	5.4	Q^3(0Al), $(SiO)_3SiOH$
After hydrothermal treatment in 0.01 M HNO_3 solution			
−97.3	238	54.4	Q^3(0Al), $(SiO)_3SiO^-$
−95.4	113	7.4	Q^3(0Al)*
−94.1	211	30.3	Q^3(0Al)
−85.4	247	7.9	Q^3(0Al), $(SiO)_3SiOH$

Table 4. ^{29}Si chemical shift, FWHM, and area under the curve of the different contributions obtained from the fitting of the ^{29}Si MAS NMR spectrum of saponite and vermiculite eucatex.

δ (ppm)	FWHM (Hz)	%	Phase
Saponite			
Starting material			
−95.8	211	67.9	Q^3(0Al)
−90.8	204	30.6	Q^3(1Al)
−85.0	199	1.5	Q^3(2Al)
After hydrothermal treatment in water			
−95.8	258	70.4	Q^3(0Al)
−90.9	249	29.3	Q^3(1Al)
−85.0	199	0.3	Q^3(2Al)
After hydrothermal treatment in 0.01 M HNO_3 solution			
−95.4	208	68.4	Q^3(0Al)
−90.5	196	29.1	Q^3(1Al)
−85.0	199	2.5	Q^3(2Al)
Vermiculite eucatex			
Starting material			
−99.6	2872	40.0	Q^4(0Al), $(SiO)_4SiOH$
−93.4	549	8.8	Q^3(0Al)
−88.6	590	40.5	Q^3(1Al)
−84.2	679	10.6	Q^3(2Al)
After hydrothermal treatment in water			
−106.8	3815	65.4	Q^4(0Al), $(SiO)_4SiOH$
−93.4	778	23.2	Q^3(0Al)
−88.6	461	11.5	Q^3(1Al)
After hydrothermal treatment in 0.01 M HNO_3 solution			
−97.1	5125	48.3	Q^4(0Al), $(SiO)_4SiOH$
−93.4	620	19.1	Q^3(0Al)
−88.6	542	19.1	Q^3(1Al)
−84.2	922	13.5	Q^3(2Al)

https://doi.org/10.1346/CCMN.2010.0580405 Published online by Cambridge University Press

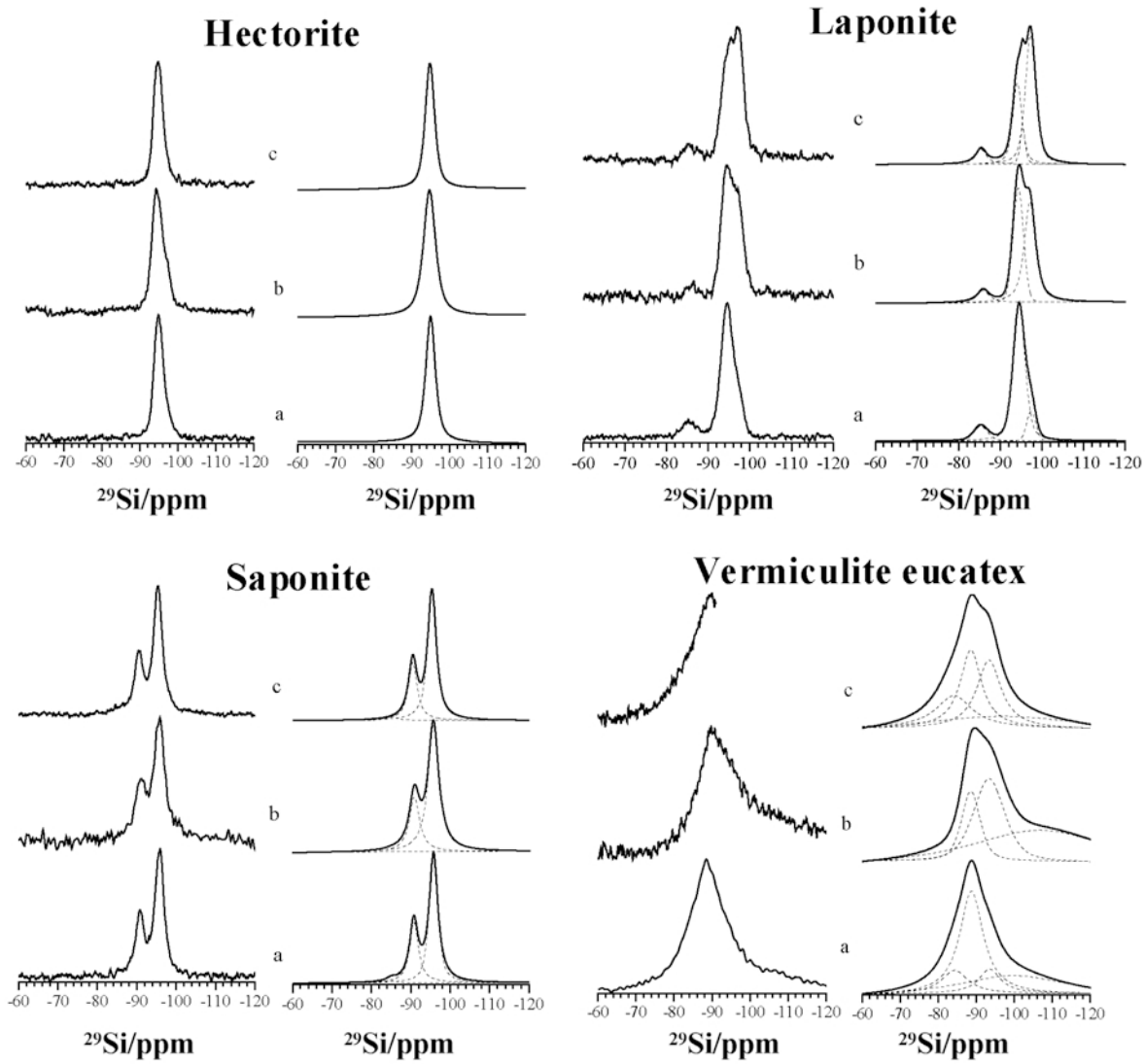

Figure 5. ^{29}Si MAS NMR spectra and fits of hectorite, Laponite®, saponite, and vermiculite eucatex: (a) starting materials, and after hydrothermal treatment at 300ºC for 48 h in two different chemical media; (b) water, and (c) 0.01 M HNO_3 solution.

The ^{27}Al MAS NMR study was only carried out for the aluminum silicates, saponite and vermiculite (Figure 6). Both of these silicates showed unique signals at ~60 ppm due to tetrahedral Al (Engelhardt and Michel, 1987). The hydrothermal treatments of vermiculite resulted in the appearance of a new signal at ~0 ppm due to octahedral Al (Engelhardt and Michel, 1987). This signal was more intense for the acid treatment, as a result of the Al leaching from the tetrahedral sheet. No changes were seen as a result of hydrothermal treatments of the saponite sample.

The ^{1}H MAS NMR spectra of the untreated smectites (Figure 7) showed two well resolved peaks, one in the range 0.30−0.65 ppm, which was assigned to framework hydroxyl groups, and the other in the range 3.70−4.30 ppm, which was assigned to interlayer water. The position of both signals depended on the chemical composition of the smectite (Alba *et al.*, 2003). Hydrothermal treatments in acidic medium resulted in a shift of the hydroxyl signal to greater frequency, as observed previously when vacancies in the octahedral sheet were produced by leaching of framework cations (Alba *et al.*, 2003). The acid treatment also caused the water signal to shift to a greater frequency due to replacement of the Na^{+} or Ca^{2+} interlayer cation by framework Mg^{2+} or Al^{3+} (Alba *et al.*, 2003). The ^{1}H MAS NMR spectra of the untreated and treated vermiculite did not allow the two expected proton environments to be resolved due to the amount of paramagnetic impurities present in the silicate, thus, these spectra were of little analytical value.

Textural analysis of the samples revealed that the lamellar aspect of the particles (Figures 8a, 9a) was

https://doi.org/10.1346/CCMN.2010.0580405 Published online by Cambridge University Press

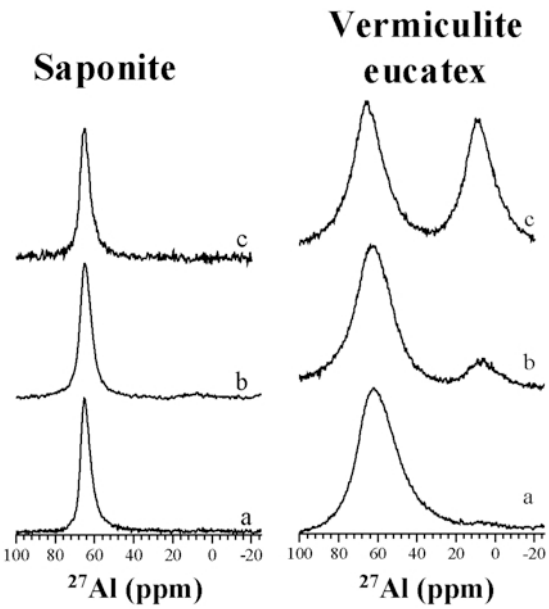

Figure 6. ^{27}Al MAS NMR spectra of saponite and vermiculite eucatex: (a) starting materials, and after hydrothermal treatment at 300ºC for 48 h in two different chemical media; (b) water; and (c) 0.01 M HNO_3 solution.

maintained after both hydrothermal treatments. The untreated samples showed EDX spectra (Figures 8b, 9b) with emission lines characteristic of the elements found in their chemical composition. Hydrothermal treatment in water (Figures 8c, 9c) resulted in a decrease in the Na and Ca line intensities. These signals disappeared completely after acid treatment (Figures 8d, 9d), and a slight decrease in the intensity of the Mg line was also observed.

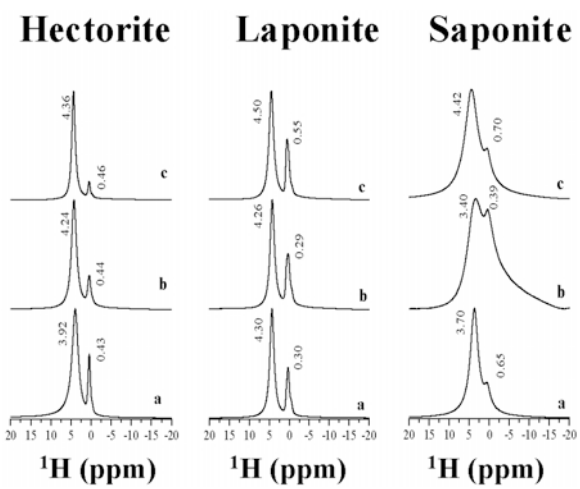

Figure 7. ^{1}H MAS NMR spectra of hectorite, Laponite®, and saponite: (a) starting materials, and after hydrothermal treatment at 300ºC for 48 h in two different chemical media; (b) water; and (c) 0.01 M HNO_3 solution.

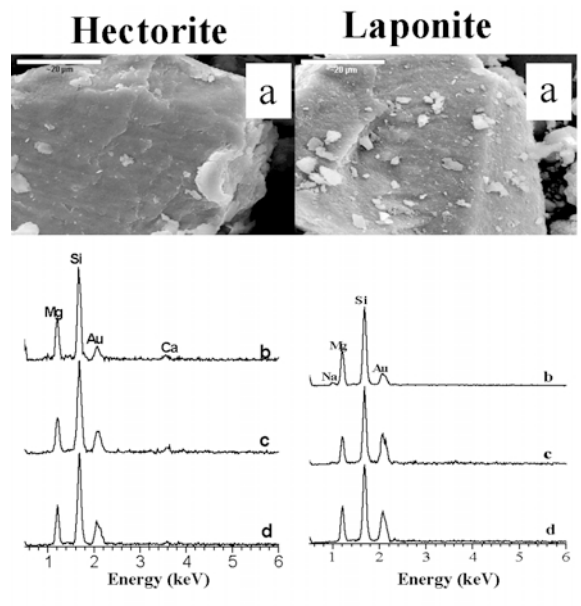

Figure 8. (a) SEM images of the starting materials and EDX spectra of: (b) starting materials, and after hydrothermal treatment at 300ºC for 48 h in two different chemical media; (c) water; and (d) 0.01 M HNO_3 solution of hectorite and Laponite®

DISCUSSION

The XRD, NMR, and SEM/EDX results demonstrated that the 1:1 and 2:1 phyllosilicates were hydrothermally

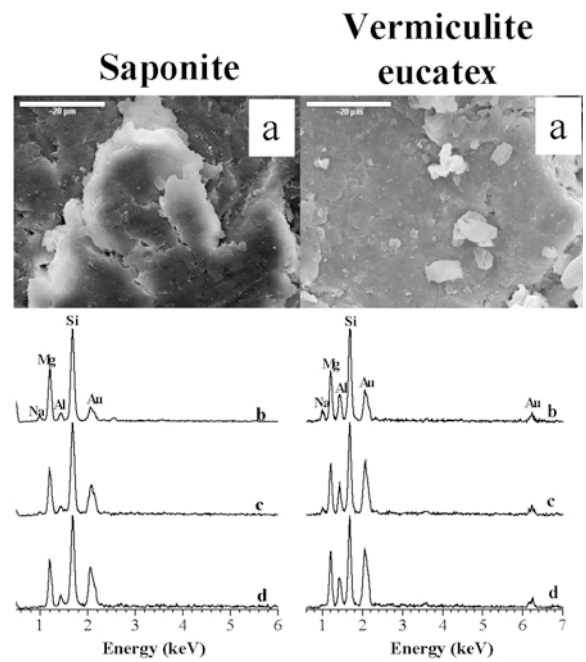

Figure 9. (a) SEM images of the starting materials and EDX spectra of: (b) starting materials, and after hydrothermal treatment at 300ºC for 48 h in two different chemical media; (c) water; and (d) 0.01 M HNO_3 solution of saponite and vermiculite eucatex.

https://doi.org/10.1346/CCMN.2010.0580405 Published online by Cambridge University Press

more stable than the 1:0 phyllosilicate. Thus, whereas total conversion of the 1:0 phyllosilicate (kanemite) to cristobalite and tridymite was observed, the long-range order of phyllosilicates containing stacked octahedral and tetrahedral sheets was maintained and only a partial transformation of pyrophyllite to boehmite was observed. The main effect of the treatments in these phyllosilicates was, in general, a locally increased disorder; the generation of new silicate phases in kaolinite, framework Mg^{2+} leaching in kaolinite, and limited transformation of Si environments from Q^3 to Q^4 in talc. The single silica sheet of 1:0 phyllosilicates confers a high flexibility to the structure, thus favoring the condensation of its Q^3 to Q^4 environments after both hydrothermal treatments.

A direct relationship between hydrothermal stability and the degree of occupancy of the octahedral sheet was observed for the 2:1 phyllosilicates with the trioctahedral member being more stable than the dioctahedral one as the partial occupancy of the octahedral sheet acts as a structural defect.

In general, hydrothermal treatment in water produced less noticeable changes in the charged 2:1 phyllosilicates than did the acid treatment. Thus, treatment in water resulted in increased short-range disorder, whereas framework cation leaching was greater in the acidic medium. Saponite showed the greatest degree of hydrothermal stability among all the smectites studied, followed by hectorite and Laponite®. The dehydroxylation of the octahedral sheet in hectorite and a significant increase in structural defects in Laponite® should be noted. The following differentiating factors support these results. (1) Li^+ in the octahedral sheet leaches more easily than Mg^{2+}, which in turn leaches more easily than Al^{3+} in the tetrahedral sheet. Isomorphic substitutions in the octahedral sheet, therefore, weaken the structure in a hydrothermal environment. (2) A smaller particle size favors a larger number of structural defects, which explains the lesser stability of Laponite® as compared to hectorite. The reactivity of the solids increases as the particle size diminishes as a consequence of an increased contact surface with the reagent. (3) A comparison of saponite and vermiculte, both of which contain tetrahedral isomorphic substitutions, showed that saponite was more stable than vermiculite as leaching of tetrahedral Al is favored by the increased isomorphic substitutions of Al for Si in this sheet (Jozefaciuk and Bowanko, 2002). This is due to the lesser strength of the Al−O bond than the Si−O bonds (Stein and Spera, 1993).

CONCLUSIONS

All the layered silicates studied, except kanemite, remained intact after hydrothermal treatment in water and with only minor structural changes being observed after hydrothermal treatment in acid. The extent of these structural changes depended on the presence or not of an octahedral sheet and the degree of occupancy of this sheet. Thus, the 1:1 and 2:1 phyllosilicates were much more stable than kanemite, which contains no octahedral sheet, and the 2:1 phyllosilicates (talc being more stable than pyrophyllite) were hydrothermally more stable than the 1:1 phyllosilicate. The absence of an octahedral sheet in the framework resulted, therefore, in less stability under the conditions of this study. In addition, the octahedral vacancies in dioctahedral silicates could be considered to be structural defects.

As for the layer-charge location, saponite was observed to be hydrothermally more stable than hectorite and Laponite®, suggesting that a tetrahedral location of the layer charge conferred greater stability than an octahedral location. Isomporphic substitution of Al for Si in the tetrahedral sheet weakened the structure , which was why saponite was more stable than vermiculite.

In the context of engineered-barrier safety, the structure of the selected bentonite must fulfill the following conditions: 2:1 layer stacking with complete occupancy of the octahedral sheet, the absence of octahedral isomorphic substitution, and a moderate tetrahedral isomorphic substitution of Al for Si. These requirements provide good hydrothermal stability and ensure appropriate water adsorption, which allows the layers to swell and seal any fissures around the canister. Saponite is the only one of the phyllosilicates analyzed here which fulfills all of these requirements.

ACKNOWLEDGMENTS

Financial support from DGICYT and FEDER Project no. CTQ2007-63297, Junta de Andalucía Project no. P06-FQM-02179, Ministerio del Medio Ambiente y Medio Rural y Marino project no. 300/PC08/3-01.1, and from EC for the project funded within the 6th Framework Program as an HRM Activity under contract number MRTN-CT-2006-035957 is acknowledged. The authors are grateful to the X-ray Laboratory and Microscopy Service at CITIUS (University of Seville, Spain) for their technical assistance.

REFERENCES

Adams, J.M. (1987) Synthetic organic chemistry using pillared, cation-exchanged and acid treated montmorillonite catalysts − A review. *Applied Clay Science*, **2**, 309−342.

Alba, M.D. and Chain, P. (2007) Persistence of lutetium disilicate. *Applied Geochemistry*, **22**, 192−201.

Alba, M.D., Becerro, A.I., Castro, M.A., and Perdigón, A.C. (2001a) Hydrothermal reactivity of Lu-saturated smectites: Part I. A long-range order study. *American Mineralogist*, **86**, 115−123.

Alba, M.D., Becerro, A.I., Castro, M.A., and Perdigón, A.C. (2001b) Hydrothermal reactivity of Lu-saturated smectites: Part II. A short-range order study. *American Mineralogist*, **86**, 124−131.

Alba, M.D., Becerro, A.I., Castro, M.A., Perdigón, A.C., and Trillo, J.M. (2003) Inherent acidity of aqua metal ions in solids: assay in layered aluminosilicates. *Journal of Physical Chemistry B*, **107**, 3996−4001.

Alba, M.D., Chain, P., and Pavón, E. (2006) Synthesis and characterization of gallium containing kanemite.

Microporous and Mesoporous Materials, **94**, 66–73.
Allen, C.C. and Wood, M.I. (1988) Bentonite in nuclear waste disposal: A review of research in support of the basalt waste isolation project. *Applied Clay Science*, **3**, 11–30.
Ames, L.L., Sand, L.B., and Goldich, S.S. (1958) A contribution on the Hector, California bentonite deposit. *Economic Geology*, **53**, 22–37.
Bauer, A, Schäfer, T., Dohrmann, R., Hoffmann, H., and Kim, J.I. (2001) Smectite stability in acid salt solutions and the fate of Eu, Th, and U in solution. *Clay Minerals*, **36**, 93–103.
Bentabol, M., Cruz, M.D.R., Huerta, F.J., and Linares, J. (2003) Hydrothermal transformation of kaolinite at 200 and 300 degrees C. *Clay Minerals*, **38**, 161–172.
Bergaya, F., Theng, B.K.G., and Lagaly, G. (editors) (2006) *Handbook of Clay Science.* Developments in Clay Science, **1**. Elsevier, New York.
Blasco, T., Corma, A., Navarro, M.T., and Pariente, J.P. (1995) Synthesis, characterization, and catalytic activity of Ti-MCM-41 structures. *Journal of Catalysis*, **156**, 65–74.
Breen, C. (1988) The acidity of trivalent cation-exchanged montmorillonite. II. Desorption of mono- and di-substituted pyridines. *Clay Minerals*, **23**, 323–328.
Breen, C. (1991a) Thermogravimetric study of the desorption of cyclohexylamine and pyridine from an acid treated Wyoming bentonite. *Clay Minerals*, **26**, 473–486.
Breen, C. (1991b) Thermogravimetric and infrared study of the desorption of butylamine, cyclohexylamine and pyridine from Ni- and Co-exchanged montmorillonite. *Clay Minerals*, **26**, 487–496.
Breen, C., Deane, A.T., and Flynn, J.J. (1987) The acidity of trivalent cation-exchanged montmorillonite. Temperature-programmed desorption and infrared studies of pyridine and n-butylamine. *Clay Minerals*, **22**, 169–178.
Cetisli, H. and Gedikbey, T. (1990) Dissolution kinetics of sepiolite from Eskisehir (Turkey) in hydrochloric and nitric acids. *Clay Minerals*, **25**, 207–215.
Čičel, B. and Novák, I. (1977) Dissolution of smectites in HCI: I. Half-time of dissolution as a measure of reaction rate. *Proceedings of the 7th Conference on Clay Mineralogy and Petrology, Karlovy Vary, Czech Republic*, pp. 163–171.
Čičel, B., Novák, I., and Pivovarníček, F. (1965) Dissolution of montmorillonites in HCI and its possible application in the study of their activation. *Silikcity*, **9**, 130–139.
Corma, A., Mifsud, A., and Sanz E. (1987) Influence of the chemical composition and textural characteristic of palygorskite on the acid leaching of octahedral cations. *Clay Minerals*, **22**, 225–232.
Corma, A., Mifsud, A., and Sanz, E. (1990) Kinetics of the acid leaching of palygorskite: Influence of the octahedral sheet composition. *Clay Minerals*, **25**, 197–205.
Cuadros, J. (2008) Clays as sealing material in nuclear waste repositories. *Geology Today*, **24**, 90–103.
Engelhardt, G. and Michel, D. (editors) (1987) *High-resolution Solid-State NMR of Silicates and Zeolites*. John Wiley & Sons, New York.
Fahn, R (1973) Influence of the structure and morphology of bleaching earths on their bleaching action on oils and fats. *Fette, Seifen, Anstrichmit.* **7**5, 77–82.
Fahn, R. and Fenderl, K. (1983) Reaction products of organic dye molecules with acid treated montmorillonite. *Clay Minerals*, **18**, 447–458.
García, M., Gancedo, J.I., Marco, J.F., Franco, M.J., Mendioroz, S., and Pajares J.A. (1989) Mössbauer study of iron removal in a montmorillonite. *Hyperfine Interactions*, **46**, 629–634.
Glasser, F.P. (2001) Mineralogical aspects of cement in radioactive waste disposal. *Mineralogical Magazine*, **65**, 621–633.
Gregor, M. and Čičel, B. (1969) Bleaching earth. Pp. 218–254 in: *Bentonite and its Application.* Publishing House SAS, Bratislava, Czech Republic.
Grim, R.E. (1968) *Clay Mineralogy*, 2nd edition. McGraw Hill, New York.
Grim, R.E. and Güven, N. (1978) *Bentonites – Geology, Mineralogy, Properties and Uses*. Developments in Sedimentology, **24**. Elsevier, New York.
Güler, C. and Sarier, N. (1990) Kinetics of the thermal dehydration of acid-activated montmorillonite by the rising temperature technique. *Thermochimica Acta*, **159**, 29–33.
Jennings, S. and Thompson, G.R. (1986) Diagenesis of Plio-Pleistocene sediments of the Colorado River Delta, southern California. *Journal of Sedimentary Petrology*, **56**, 89–98.
Johan, Z. and Maglione, G.F. (1972) Kanemite a new hydrated sodium silicate. *Bulletin de la Societé Française Mineralogie et de Cristallographie*, **95**, 371–382
Jovanovič, N. and Janačkovič, J. (1991) Pore structure and adsorption properties of an acid activated bentonite. *Applied Clay Science*, **6**, 59–68.
Jozefaciuk, G. and Bowanko, G. (2002) Effect of acid and alkali treatments on surface areas and adsorption energies of selected minerals. *Clays and Clay Minerals*, **50**, 771–783.
Laporte Industries Ltd. (1990) *Laponite Technological Bulletin*, L104/90/A, 1.
Levitz, P., Lecolier, E., Mourchid, A., Delville, A., and Lyonnard, S. (2000) Liquid-solid transition of laponite suspension at very low ionic strength: Long-range electrostatic stabilization of anisotropic colloids. *Europhysics Letters*, **49**, 672–677.
Luce, R.W. and Parks, G.A. (1972) Dissolution kinetics of magnesium silicates. *Geochimica et Cosmochimica Acta*, **36**, 35–50.
Mantovani, M., Escudero, A., Alba, M.D., and Becerro, A.I. (2009) Stability of phyllosilicates in Ca(OH)2 solution: Influence of layer nature, octahedral occupation, presence of tetrahedral Al and degree of crystallinity. *Applied Geochemistry*, **24**, 1251–1260
Massiot, D., Fayon, F., Capron, M., King, I., Le Calvé, S., Alonso, B., Durand, J.O., Bujoli, B., Gan, Z., and Hoatson, G. (2002) Modelling one- and two-dimensional solid-state NMR spectra. *Magnetic Resonance in Chemistry*, **40**, 70–76.
Mather, J.D., Chapman, N.A., Black, J.H., and Lintern, B.C. (1982) The geological disposal of high-level radioactive waste – a review of the Institute of Geological Sciences Research programme. *Nuclear Energy*, **21**, 167–173.
Morgan, D.A., Shaw, D.B., Sidebottom, M.J., Soon, T.C., and Taylor, R.S. (1985) The function of bleaching earths in the processing of palm, palm kernel and coconut oil. *Journal of the American Oil Chemical Society*, **62**, 292–299.
Murray, H.H. (1991) Overview – Clay Mineral Applications. *Applied Clay Science*, **29**, 379–395.
Murray, H.H. (1999) Applied clay mineralogy today and tomorrow. *Clay Minerals*, **34**, 39–49.
Murray, H.H. (2000) Traditional and new applications for kaolin, smectite, and palygorskite: a general overview. *Applied Clay Science.*, **17**, 207–221.
Nagy, K.L. (1995) Dissolution and precipitation kinetics of sheet silicates. Pp. 173–225 in: *Chemical Weathering Rates of Silicate Weathering* (F.W. White and S.L. Brantley, editors). Reviews in Mineralogy, **31**. Mineralogical Society of America, Washington, D.C.
Novák, I. and Čičel, B. (1978) Dissolution of smectites in HCl: II. Dissolution rate as a function of crystallochemical composition. *Clays and Clay Minerals*, **26**, 341–344.
Petit, S., Martin, F., Wiewióra, A., De Parseval, P., and Decarreau, A. (2004) Crystal-chemistry of talc: A near infrared (NIR) spectroscopy study. *American Mineralogist*,

89, 319–326.
Prost, J.L. (1984) Saponite from near Ballarat, California. *Clays and Clay Minerals*, **32**, 147–153.
Pusch, R. and Yong, R. (2003) Water saturation and retention of hydrophilic clay buffer-microstructural aspects. *Applied Clay Science*, **23**, 61–68.
Pusch, R., Zwahr, H., Gerber, R., and Schomburg, J. (2003) Interaction of cement and smectite clay – theory and practice. *Applied Clay Science*, **23**, 203–210
Pusch, R., Kasbohm, J., Pakovsky, J., and Cechova, Z. (2007) Are all smectite clays suitable as "buffers". *Physics and Chemistry of the Earth*, **32**, 116–122.
Ramírez, S., Cuevas, J., Vigil, R., and Leguey, S. (2002) Hydrothermal alteration of ''La Serrata'' bentonite (Almería, Spain) by alkaline solutions. *Applied Clay Science*, **21**, 257–269.
Read, D., Glasser, F.P., Ayora, C., Guardiola, M.T., and Sneyers, A. (2001) Mineralogical and microstructural changes accompanying the interaction of boom clay with ordinary Portland cement. *Advanced Cement Research*, **13**, 175–183.
Sánchez-Soto, P.J., Justo, A., and Pérez-Rodríguez, J.L. (1994) Grinding effect on kaolinite-pyrophyllite-illite natural mixtures and its influence on mullite formation. *Journal of Materials Science*, **29**, 1276–1283.
Sanz, J. and Serratosa, J.M. (1984) Si-29 and Al-27 High-Resolution MAS-NMR spectra of phyllosilicates. *Journal of the American Chemical Society*, **106**, 4790–4793.
Savage, D. and Chapman, N.A. (1982) Hydrothermal behaviour of simulated waste glass- and waste-rock interaction under repository conditions. *Chemical Geology*, **36**, 59–86.
Savage, D., Noy, D., and Mihara, M. (2002) Modelling the interaction of bentonite with hyperalkaline fluids. *Applied Geochemistry*, **17**, 207–223.
Siddiqui, M.K.H. (1968) *Bleaching Earths.* Pergamon Press, Oxford, UK, 86 pp.
Stein, D.J. and Spera, F.J. (1993) Experimental rheometry of melts and supercooled liquids in the system $NaAlSiO_4$-SiO_2-Implications for structure and dynamics. *American Mineralogist*, **78**, 710–723.
Weiss, C.A, Altaner, S.P., and Kirkpatrick, R.J. (1987) High-resolution ^{29}Si NMR spectroscopy of 2:1 layer silicates: Correlations among chemical shift, structural distortions, and chemical variations. *American Mineralogist*, **72**, 935–942.
Wheeler, P.A., Wang, J., Baker, J., and Mathias, L.J. (2005) Synthesis and characterization of covalently functionalized Laponite clay. *Chemistry and Materials*, **17**, 3012–3018.
White, G.N., Dixon, J.B., Weaver, R.M., and Kunkle, A.C. (1992) Sedimentary structure in gray kaolins of Georgia. *Clays and Clay Minerals*, **40**, 555–560.
Williams-Daryn, S., Thomas, R.K., Castro, M.A., and Becerro, A. (2002) The structures of complexes of a vermiculite intercalated by cationic surfactants, a mixture of cationic surfactants, and a mixture of cationic and non-ionic surfactants. *Journal of Colloid and Interface Science*, **256**, 314–324.

(*Received 4 June 2009; revised 28 May 2010; Ms. 322; A.E. M.A. Velbel*)